# Three-Axis Capacitive Touch-Force Sensor for Clinical Breast Examination Simulators

Jayer Fernandes, *Student Member, IEEE*, and Hongrui Jiang, *Fellow, IEEE*

***Abstract*— Clinical breast examinations (CBEs) are a vital part of breast cancer screening programs. However, there is a lack of standardization in the kinds of motion and the forces used during the examination, which can lead to either an inaccurate or a missed diagnosis. The use of sensors in CBE simulations and training can help to alleviate this issue. This paper demonstrates a flexible, three-axis capacitive touch-force sensor that utilizes a patterned elastomeric dielectric layer. The sensor was fabricated from a copper-clad Kapton laminate and can resolve normal pressure and track directional motion. The electronic and mechanical properties of the patterned dielectric layer were analyzed in detail using finite-element analysis techniques and these results were then used to optimize the sensor. In a mock CBE setup, we used a breast model to demonstrate that the sensor, when placed under the model, could track a normal force of about 18 N when applied to the test area, as well as the trajectory of the force as it was applied around the breast model. This data, along with the accompanying variations in signal patterns, can be utilized to quantify the CBE conducted by an expert physician, which in turn can be used as feedback in training tools for residents and other physicians.**

***Index Terms*— Flexible printed electronics, capacitive sensing, motion sensor, tactile sensing, clinical breast examination, soft-lithography.**

## I. Introduction

BREAST cancer is the second leading cause of cancer related deaths amongst women in the United States [1]. Early and adequate screening can play a significant role in improving patient outcomes in the areas of mortality reduction and improved life-years gained. One of the widely recognized approaches to breast cancer screening is CBE, which is considered to be a vital early detection and prevention tool amongst women who do not receive regular mammograms [2].

CBE primarily depends on the visual inspection and palpation of the breast and the surrounding tissue with a particular series of motions (shown in Fig. 1) that are designed to determine and distinguish between lumps and nodules to determine their extent and boundaries, as well as their depth, mobility and density - information that is vital to its determination of being either benign or malignant [3]. Despite the fact that the CBE is a recommended component of a comprehensive screening platform and that it is performed by a large number of physicians in the U.S., the manner in which it is performed varies considerably between physicians and there is no standardization of the techniques used [4]. It has been observed that training studies using objective and structured clinical examinations have clear improvements in the performance of CBE techniques and patient interaction skills [5]. Studies using silicone breast models show that both training in CBE technique and experience in detecting breast lumps can increase the sensitivity for detecting lumps in the models [6]. It has also been shown that training with silicone breast models increases the detection of known benign lumps in women, clearly indicating that the improvement in detection skills can be applied to patients [7].

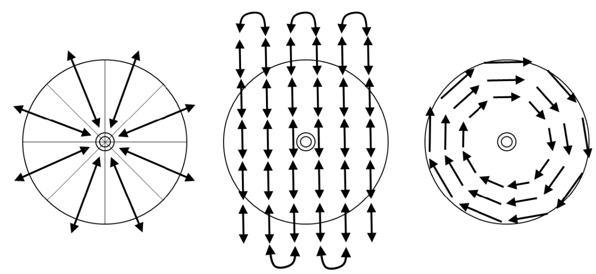


Fig. 1. Schematics exhibiting some of the different kinds of hand palpations that are commonly used during a CBE. Each of these motions is geared towards identifying the location, extent and depth of the mass and its boundaries.

Medical students and residents have been observed to achieve low performance scores on objective examinations of the CBE components, as well as low sensitivity and specificity using silicone breast models, illustrating the limitations of the current tools and methods used in medical school training [8]. This lack of standardization of the techniques and the forces involved in CBE has significant repercussions. It is known that there is a strong correlation between the amount of force used during a CBE palpation and the accuracy in the detection of lesions [9]. Specifically, it was observed that reduced palpation forces that were less than 10N placed physicians at the risk of missing deep tissue lesions near the chest wall. There is thus a strong need for the development of better CBE training simulators and sensors to provide physicians and residents with real time and quantitative feedback in order to improve their CBE techniques.

The use of sensors in CBE simulations can help characterize and standardize CBE techniques with a level of detail that

Manuscript received March 6, 2017; revised July 19, 2017; accepted July 24, 2017. Date of publication July 31, 2017; date of current version October 24, 2017. This work was supported by H. Jiang's Vilas Distinguished Achievement Professorship and Lynn H. Matthias Professorship, and Wisconsin Alumni Research Foundation (WARF). An earlier version of this paper was presented at the IEEE SENSORS 2016 Conference and was published in its Proceedings. The associate editor coordinating the review of this paper and approving it for publication was Prof. Ravinder S. Dahiya. *(Corresponding author: Hongrui Jiang.)*

J. Fernandes is with the Department of Electrical and Computer Engineering, University of Wisconsin–Madison, Madison, WI 53706 USA (e-mail: jfernandes@wisc.edu).

H. Jiang is with the Department of Electrical and Computer Engineering, the Department of Biomedical Engineering, the Department of Materials Science and Engineering, the Department of Ophthalmology and Visual Sciences, and the McPherson Eye Research Institute, University of Wisconsin–Madison, Madison, WI 53706 USA (e-mail: hongrui@engr.wisc.edu).

Digital Object Identifier 10.1109/JSEN.2017.2733762

is not possible through mere observation alone [9]. It is imperative that any potential sensing solution should be capable of measuring both shear and normal forces, in order to measure the applied pressure as well as to track the trajectory of the applied forces [10]. Currently, the sensing solutions proposed are based on piezoelectric sensing schemes and can measure only normal pressure over a large area, but not directional changes. As a result, they are incapable of tracking the motions used during CBE palpations, which are critical to determining the size of a lump. They also show hysteresis and are susceptible to drift as a result of temperature variations and external vibrations [11]. A capacitive sensing solution is preferred because of its high sensitivity, low power consumption and low drift. Prior work in the area of flexible capacitive sensors has mainly focused on soft and compliant tactile sensors for robotic tactile sensing, which operate at low force regimes [12]–[15].

In order to have greater control over the electronic and mechanical performance of these sensors, we have developed a novel normal and shear capacitive touch-force sensor structure with a patterned dielectric layer. We previously reported preliminary results on this sensor in [16] and here we describe the design, analysis and fabrication of these touch-force sensors in greater detail. We intensively investigated the effects of the geometry of the dielectric layer structures on the sensitivity of the device through the use of numerical simulations. The dimensions of the flexible dielectric allows us to stay in the elastic regime, while the patterned structures provide surfaces that can deform easily and allow for a quick recovery from the deformation, thus improving the response of the device to different motions. Each of the patterned dielectric posts can flex in the direction of the applied force, which allows us to measure the force and track the trajectory of the palpation through the use of an overlapping electrode geometry. These devices were fabricated using rapidly prototypable soft-lithography steps, based on casting soft polymers in 3-D printed molds. The fabricated devices were then tested under different conditions, including a mock CBE using a silicone model breast where the measurements agreed with the conclusions derived from the simulation data and showed that these devices had good sensitivity, low cross talk and low hysteresis.

## II. Sensor Design

We devised a novel capacitive sensing scheme along with a structured dielectric layer fabricated using soft-lithography, in order to realize mechanically robust and tunable touch-force sensors.

### A. Operating Principle

A capacitive sensing scheme is based on the change in capacitance between the top and bottom electrodes of a capacitor, which can be attributed to either one or more of the following – a change in the thickness of the dielectric layer (if the dielectric is sufficiently compliant), a change in the permittivity of the dielectric layer, or a change in the overlap area between the top and bottom electrode. We exploit these effects in order to develop a capacitive sensor that can detect motion both in the normal and shear directions.

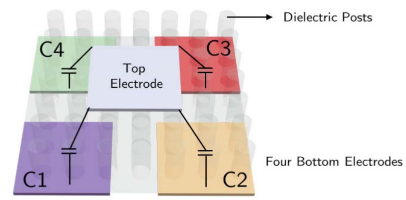


Fig. 2. A schematic of the device showing the structured dielectric layer with its posts and the four differential capacitances C1, C2, C3 and C4 formed between the top electrode and each of the four bottom electrodes.

When a normal force is applied to a capacitive sensor with a compliant dielectric layer, the thickness of the dielectric layer decreases, leading to an increase in the capacitance. When a tangential force is applied to the sensor, the dielectric layer shears in the direction of the force, resulting in a change in the overlap area between the two electrodes, which in turn causes a change in the capacitance. In many cases, shear forces have an inherent normal component to them and while the change in capacitance can largely be attributed to the change in the overlap area between the top and bottom electrode, a small fraction must be attributed to the change in thickness of the dielectric layer that accompanies the normal component.

This change in capacitance can be measured with the aid of custom readout electronics, which allows us to keep track of the trajectory of different kinds of motions as well as the corresponding forces that are used during the exam. This data can then be compared with pre-verified practitioner data, in order to provide real-time feedback to the residents in training.

### B. Sensor Design

Our sensing solution is a three-axis capacitive sensor with a structured dielectric layer, as shown in Fig. 2. There are two aspects to the design of the sensor which allow for the sensing of shear and normal motion.

The first is the design of the electrode geometry. The sensor structure consists of a central top electrode overlapping four bottom electrodes, forming four individual differential capacitors C1, C2, C3, C4. As the differential capacitors are in parallel, the total capacitance is given by the sum of the individual capacitances.

$$C_{total} = C_1 + C_2 + C_3 + C_4$$
$$C_i = \frac{\epsilon_0 \epsilon_r A_i}{d}$$

where $C_i$ is the differential capacitance between the top electrode and the i$^{th}$ bottom electrode, $\epsilon_0$ is the free space permittivity, $\epsilon_r$ is the effective permittivity of the dielectric structure, $A_i$ is the overlap area between the top electrode and the i$^{th}$ bottom electrode and $d$ is the overall thickness of the structured dielectric layer. Normal forces/motions can easily be detected by the simultaneous increase in all four differential capacitances as a result of the decrease in the thickness of the dielectric layer.

The breaking of the symmetry of the bottom electrode, with respect to the top electrode, allows for shear motion to be detected through the increase in the overlap area between the top electrode and the specific bottom electrode in the direction of the shear, and the consequent decrease in the overlap areas between the top electrode and the remaining bottom electrodes. Consequently, the differential capacitance(s) of the differential capacitor(s) in the direction of the shear motion increases, while the other differential capacitance(s) decrease. The change in the differential capacitance is given as follows

$$\Delta C_i = \frac{\epsilon_i \epsilon_r (x\Delta y + y\Delta x)}{d}$$

where $\Delta C_i$ is the change in the differential capacitance between the top electrode and the i$^{\text{th}}$ bottom electrode, $\epsilon_0$ is the free space permittivity, $\epsilon_r$ is the effective permittivity of the dielectric structure, $\Delta x$ is the change in the x-component and $\Delta y$ is the change in the y-component of the overlap area between the top electrode and the i$^{\text{th}}$ bottom electrode and $d$ is the overall thickness of the structured dielectric layer.

The second aspect is the design of the dielectric layer. The mechanical properties of the dielectric film as well as the engineering of its structure are important factors in determining the sensitivity of the touch-force sensor. A soft and compliant dielectric layer will result in a lower range of force measurements and a higher sensitivity to shear and normal motions, while a firmer dielectric layer will result in a higher range of force measurements and a lower sensitivity to shear and normal forces. In either case, a solid dielectric film has a limited ability to shear, resulting in a limited shear measurement. In addition, the deformation of an elastomeric thin film subjects it to intrinsic mechanisms, which results in long relaxation times after compression. In order to counter this, we have designed a capacitive sensor with a patterned dielectric layer measuring a few millimeters in thickness. The thickness of the flexible dielectric allows us to stay in the elastic regime, while the patterned structures provide surfaces that can deform easily in response to either a shear or a normal force, allowing for a quick recovery from the deformation, thus improving the sensitivity of the device. Each of the patterned dielectric posts can flex in the direction of the applied force, allowing us to track the trajectory of different kinds of motions.

## III. Multi-Physics Simulations

The deformation of the dielectric layer and hence the change in the differential capacitance can be tuned by varying the geometrical parameters of the dielectric layer viz. the height and width of the posts, the spacing between the posts and the geometry of the posts themselves.

In order to understand the effect of variations in the geometrical parameters of the dielectric layer on the initial capacitance and deformation maximum values respectively, we conducted 3-D, nonlinear, large-deflection finite element analysis sweeps in ANSYS 17.2. Specifically, we set up a two-way coupled simulation between the ANSYS Mechanical and ANSYS Maxwell modules and first calculated the initial capacitance of the device in ANSYS Maxwell. The results from this simulation were imported into the ANSYS Mechanical module as a Body Force Density applied to the five electrodes and a mechanical deformation was then simulated by applying a force at an angle to the top plate. The mechanically deformed structure was then imported back into Maxwell to calculate the final differential capacitance values between the top and bottom electrodes. The top and bottom substrates were made from Kapton with a dielectric permittivity of 3.5, while the intermediate dielectric layer was made from Ecoflex-30 with a dielectric permittivity of 2.5. We simulated shear forces by applying a force in the X and Y (in-plane) directions and normal forces in the Z direction. A fixed boundary condition was applied to the base of the device.

### *A. Effect of the Post Height and the Post Diameter on the Deformation and Shear Differential Capacitance*

We looked at the effect of varying the post height and the post diameter on the initial differential capacitances, as well as the overall deformation and the differential capacitances after shearing the device. Intuitively, decreasing the aspect ratio of the posts by reducing either the diameter of the posts or increasing its height allows for greater levels of shear between the top and bottom plates, resulting in a larger capacitance differential, which is a desirable feature for sensing shear forces.

Fig. 3 (a) shows the change in the deformation of the top plate with respect to the bottom plate as a function of the post height and diameter. From the simulation results, we see that there is a strong correlation between the reduction in the aspect ratio of the posts and the maximum amount of deformation that can be achieved. We also simulated these results for different shear force magnitudes (5N, 15N, 30N) and found that these results were consistent for all three forces, indicating that the device maintains a reliable response across a large force regime. Fig. 3 (b) shows the change in the differential capacitance between the top plate and one of the bottom electrodes in the direction of the shear force, as a function of the post diameter and post height. Comparing the simulation results for the effects of the variation in the aspect ratio on the post deformation and shear differential capacitances, we see that a reduced aspect ratio is indeed a viable route to improving the shear response, as it allows for a larger deformation, which in turn results in a larger increase in the overlap area between the top electrode and the bottom electrode in the direction of the shear motion, allowing for a greater shear capacitance differential. This was again verified for different shear forces and the results were found to be consistent across the force regimes.

### *B. Effect of the Post Height and the Post Diameter on the Initial Differential Capacitances*

We also looked at the effect of varying the post height and the post diameter on the initial capacitance of the sensor. The capacitance of a device is inversely proportional to the separation gap between the top and bottom plates. We expect to see a decrease in all the four differential capacitances as the height of the posts is increased. A high initial capacitance is beneficial for normal force sensing. However, a larger post height also allows us the benefit of a larger range of compression in the normal direction, which results in a higher sensitivity to normal forces. Hence, there exists an application specific trade-off between the value of the initial capacitance and the sensitivity of the device with respect to the post height.

Fig. 4 (a) and Fig. 4 (b) show the simulation results for the initial capacitance as a function of the post height and post

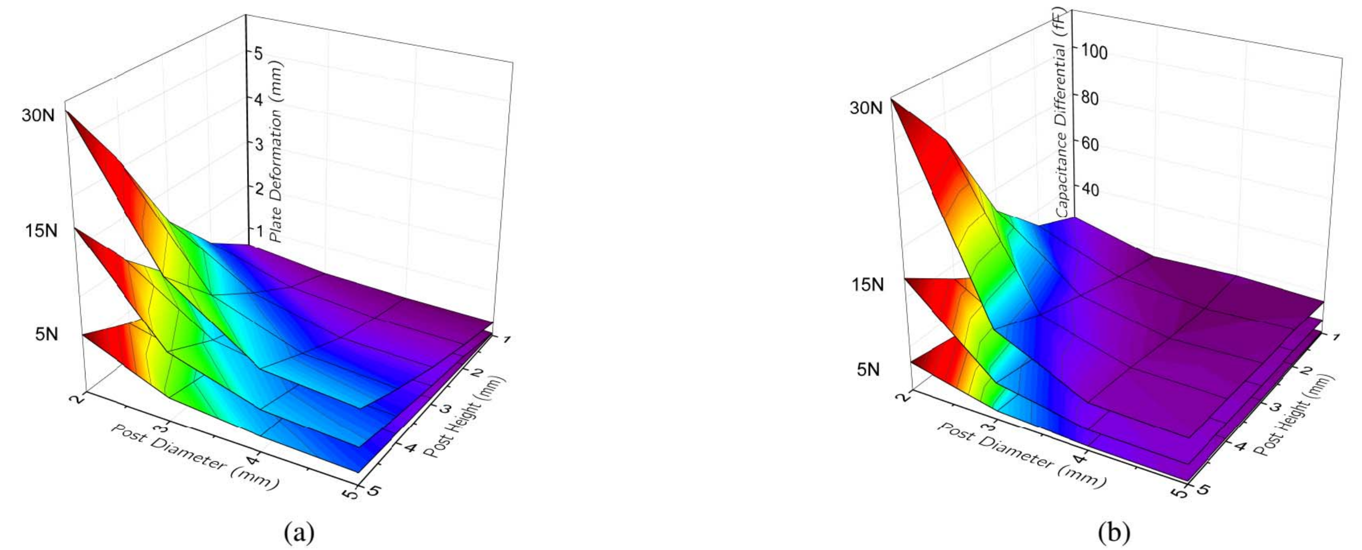


Fig. 3. (a) Change in the deformation of the top plate as a function of the post height and the post diameter, for three different forces i.e. 5N, 15N and 30N. (b) Change in the differential capacitance of a single differential capacitor in the direction of the shear force as a function of the post height and the post diameter, for three different forces i.e. 5N, 15N and 30N.

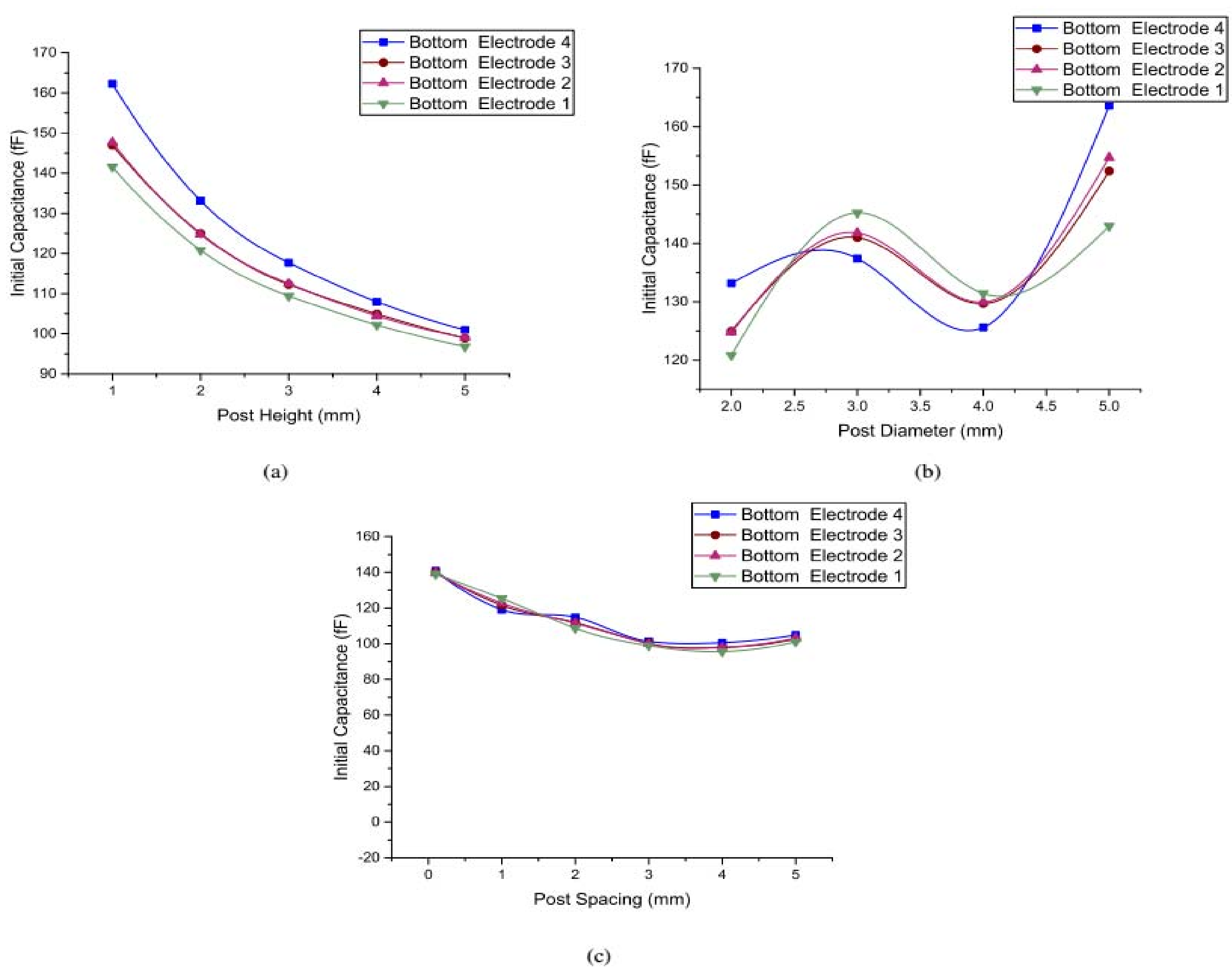


Fig. 4. (a) Variation in the initial differential capacitances of the sensor with the post height, for a fixed post diameter of 2mm. (b) Variation in the initial differential capacitances of the sensor with the post diameter, for a fixed post height of 2mm. (c) Variation in the initial differential capacitances of the sensor with the post spacing, for a fixed post diameter of 3mm and a post height of 4mm.

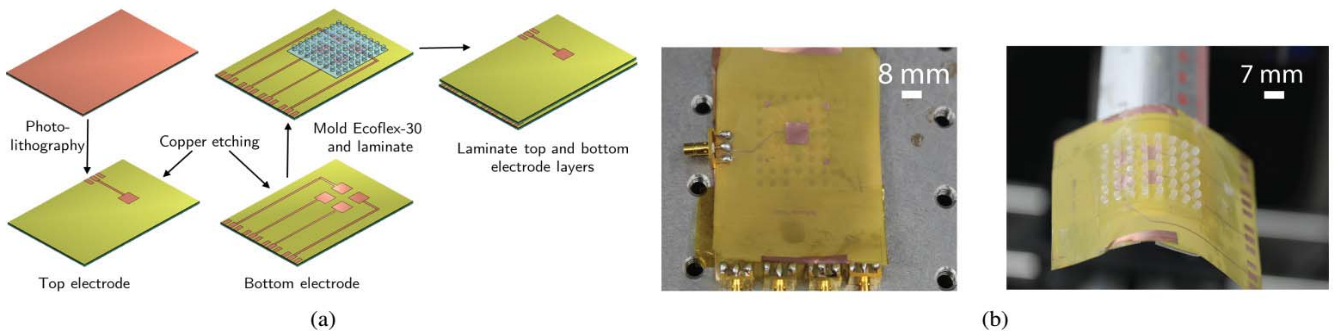


Fig. 5. (a) Schematic of the fabrication of the flexible touch-force sensor - From left, the top and bottom electrodes are defined on Kapton using standard photolithography techniques. Next, the patterned dielectric layer is fabricated using soft lithography. Finally, the top and bottom layers are laminated to complete the sensor. (b) Fabricated touch-force sensor with 7 mm by 7 mm plate size, 4 mm spacing between plates (left). The patterned dielectric posts laminated to the bottom layer as well as the flexibility of the device are shown on the right.

diameter. As expected, there is a strong monotonic decrease in the initial differential capacitances with an increase in the post height. It is also observed that there are small non-monotonic increases in the initial differential capacitances with an increase in diameter (while ensuring that the spacing between the posts is constant, in all cases). This can be attributed to the overall increase in the effective permittivity of the structured dielectric layer. As the diameter of the posts increases, the effective fill-factor of material with a larger dielectric constant increases, resulting in an overall increase in the effective permittivity of the dielectric layer.

### C. Effect of the Post Spacing on the Initial Differential Capacitances

Fig. 4 (c) shows the simulation result for the variation in the initial capacitances as a function of the spacing between the posts. For a fixed post height and post diameter, increasing or decreasing the spacing between the posts results in a corresponding increase or decrease in the four initial differential capacitances. There are two contributing factors at hand to this phenomenon. The first factor, as mentioned earlier, results from the fact that changing the spacing between the posts results in a change in the dielectric fill-factor, which in turn affects the effective permittivity of the structured dielectric layer. The second factor is the change in the number of posts between the top and bottom electrodes of each of the individual differential capacitors C1, C2, C3 and C4. Since the dielectric layer is fabricated in a manner that leads to a somewhat random positioning of the posts between the top and bottom electrodes, there are variations in the number of posts in each differential capacitor, leading to minor variations in the effective permittivity, and hence the initial capacitance of the device. These are taken into account when performing the device calibration.

## IV. Device Fabrication

Our fabrication process leverages techniques that we have previously developed [17]–[21] and soft lithography in order to rapidly prototype devices based on the specific application requirement. The approach utilizes a 3D printing based molding technique, which allows us to fabricate dielectric posts of different geometrical parameters with ease. The process includes the fabrication of separate top and bottom components that are aligned and bonded with the dielectric layer. The use of established fabrication techniques results in a high level of device reproducibility.

A brief overview of the fabrication process is shown in Fig. 5 (a) and images of the fabricated devices are shown in 5 (b). The upper and lower electrode layers were fabricated from Dupont Pyralux AC0092500EV, which is a copper-clad Kapton laminate (copper thickness $9\mu$m, polyimide thickness $25\mu$m). The Kapton laminate was first cut into rectangular pieces and then rinsed in acetone, followed by isopropyl alcohol (IPA) and then deionized (DI) water to remove any trace of oils and other contaminants. AZP4620 photoresist was spun onto the Kapton substrates at an initial speed of 500 rpm for 10 seconds, followed by a 4000 rpm cycle for 30 seconds to achieve a thickness of $6\mu$m, after which, the devices were soft baked at 115°C for 90 seconds. The copper layer was then patterned using a collimated ultraviolet (UV) light source (Omnicure Series 2000, Lumen Dynamics Group Inc., Excelitas Technologies) with a dosage of 310 mJ/cm$^2$ (10 mW/cm$^2$ for 31 seconds). The patterns were developed in a diluted AZ 400K solution (1 AZ 400K:3 DI $H_2O$) for 45 seconds. In order to define the electrodes, the copper layer was etched using copper etchant at 40°C for 12 - 15 minutes (APS-100 Copper Etchant), after which the devices were rinsed in acetone to strip the photoresist layer and then cleaned with IPA and DI water.

## V. Results and Discussion

### A. Measurement Setup

Measurements were carried out using a custom PCB designed around the AD7746 Capacitance-to-Digital IC (Analog Devices, Inc., MA, USA). The AD7746 has two channels for measuring a changing capacitance with a full scale range of ±4 pF, at a resolution of 4 aF. A 32 kHz signal was provided to the sensor by the IC, to excite the sensor and synchronize the capacitance measurements. A data update rate of 9.1 Hz was used in order to keep the noise level low and hence raise the effective resolution. Data acquisition was done through the I2C serial interface using an Arduino Uno micro-controller board.

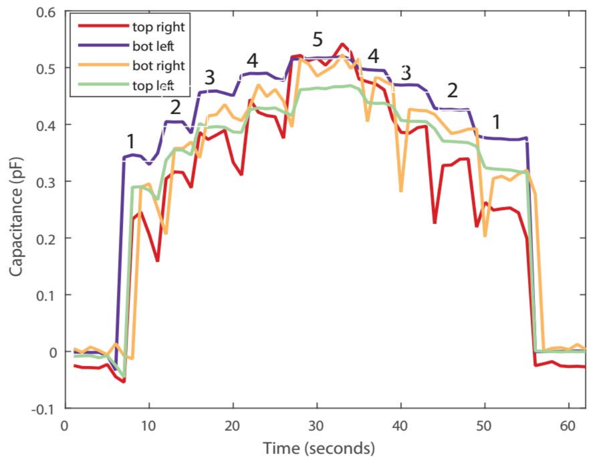


Fig. 6. Measured capacitive response of a single four-plate capacitor cell to a normal load that was increased in steps of 0.17N to 0.85N (steps 1,2,3,4,5) and then decreased (steps 5,4,3,2,1).

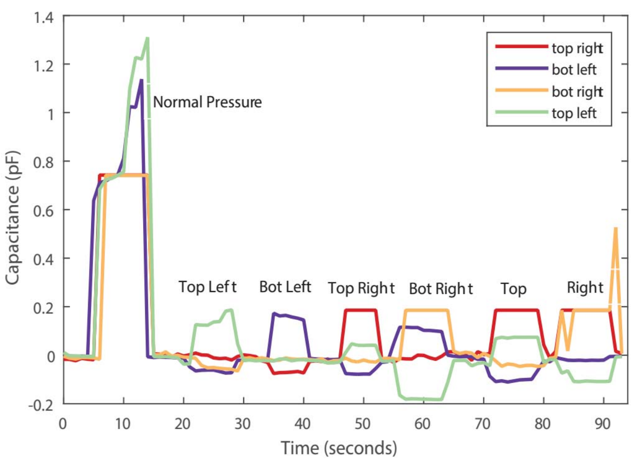


Fig. 7. Time series change in the capacitance of a single four plate capacitor cell to different pressure scenarios when the sensor was palpated by hand.

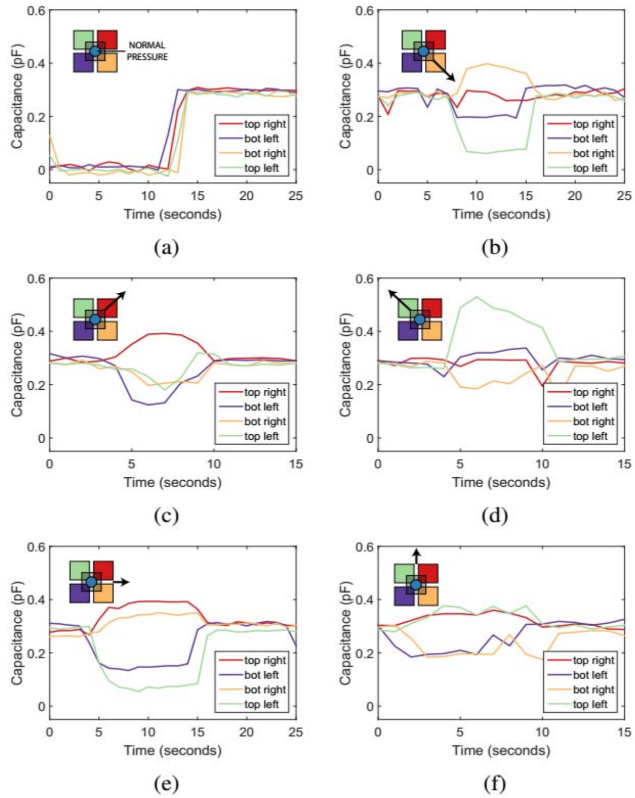


Fig. 8. Measured capacitances of a single 4 plate capacitor cell when a constant force of 0.17 N is placed on the sensor and then moved around. (a) The response of the sensor at the point when the force is applied. (b) The response of the sensor when the force is moved towards the bottom right plate. (c) The response of the sensor when the force is moved towards the top right plate. (d) The response of the sensor when the force is moved towards the top left plate. (e) The response of the sensor when the force is moved towards the right. (f) The response of the sensor when the force is moved towards the top.

### *B. Capacitance Under a Stepped Load*

In order to characterize the response of the sensor to normal pressure, 18g calibration weights were stacked incrementally (where each weight exerts approximately 0.17N of downwards force) on a device with a dielectric post height of 4 mm, post diameter of 2 mm and square electrodes of size 8 mm by 8 mm, with a 4 mm spacing in between the plates, until 0.85N, and then decreased in steps of 0.17N, as shown in Fig. 6. These post dimensions were chosen in order to optimize the sensor response, while ensuring reliable fabrication. We see a large jump in capacitance for the first increment (step 1), of the order of 250-350 fF, following which there are regular increases of 100 fF per step. This pattern can be attributed to the sudden compression of the elastomer dielectric layer posts with the initial load and gradual compression with subsequent load increments. The same response was seen when the load was removed gradually, with a small amount of hysteresis.

### *C. Three-Axis Performance*

We then palpated the same sensor directly in different directions in order to determine the response of the sensor to forces of different directions and magnitudes. As can be seen from the time series in Fig. 7, the sensor was able to generate distinct differential capacitance patterns for each of the scenarios that was simulated. In the event of a normal force, we saw a sharp rise in all the four individual differential capacitances, due to the reduction in the thickness of the dielectric layer. When a shear force was applied, the increase in overlap area of differential capacitor(s) in the direction of the shear resulted in an increase in the corresponding differential capacitance(s), while the other differential capacitor(s) showed a decrease in their overlap area and hence a decrease in their differential capacitance(s).

### *D. Simulation of Clinical Breast Examination*

In order to validate the performance of the sensor during a clinical breast examination, two different kinds of experiments were performed. In the first case, a constant force of approximately 0.17 N was applied to the sensor and then moved around after measuring the normal response, in order to track to motion. With this method, we were able to fix and calibrate the normal response, following which we began tracking the motion in different directions. Fig. 8 (a) shows the normal response of the sensor to the applied force. After

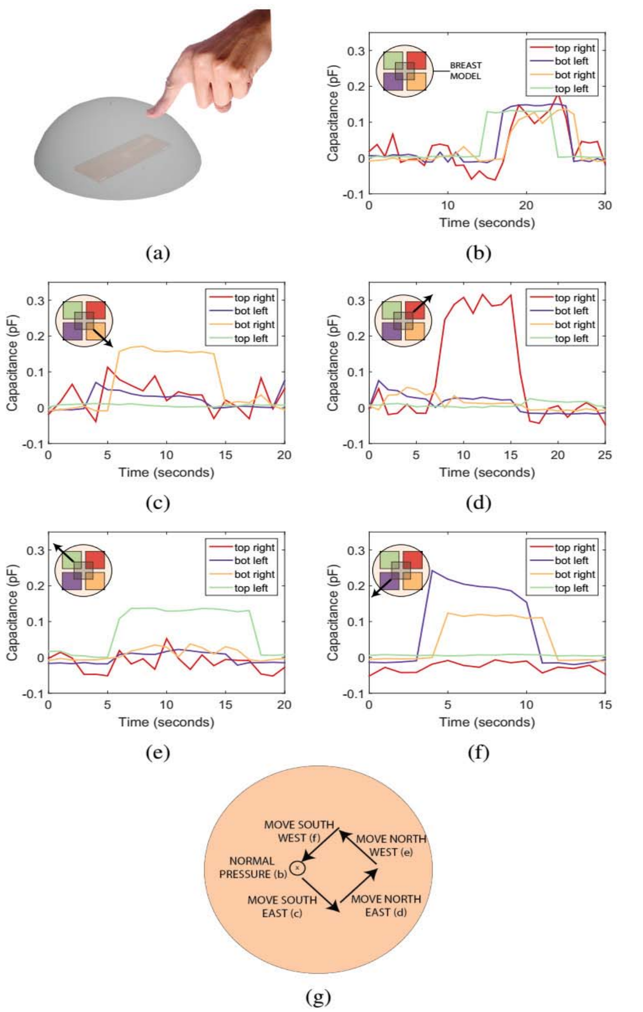


Fig. 9. Measured capacitances during a mock CBE. (a) Schematic of the examination setup. (b) The response of the sensor when a normal pressure is applied to the breast model. (c) The response of the sensor when the pressure is moved in the south-east direction. (d) The response of the sensor when the pressure is moved in the north-east direction. (e) The response of the sensor when the pressure is moved in the north-west direction. (f) The response of the sensor when the pressure is moved in the south-west direction. (g) Schematic of the trajectory of the motion around the breast from start to stop.

applying the force, the baseline capacitance shifted to 0.3 pF. Figs. 8 (b), (c), (d) show the response of the sensor, tracking motion, as we moved towards the bottom right plate, top right plate and top left plate, respectively. The dip in the capacitance values of the opposite plates was a result of the increase in the distance between the top and bottom electrodes, while the increase in capacitance was due to the increase in the overlap area between the top and bottom plates in the direction of the motion. Figs. 8 (e), (f) show the response of the sensor when we moved towards the right and top, respectively. In this case, the overlap of two plates in the direction of the motion increased, thus raising both their differential capacitance values.

In the second case, the ability of the sensor to track the trajectory of motion around a silicone breast model was verified during a mock CBE. The breast model was placed over the capacitive sensor as shown in Fig. 4 (a), following which a calibration routine was run to set the baseline capacitance to 0 pF. The breast model was then palpated in different directions with a force of about 18 N. Fig. 9 (b) shows the response of the sensor to palpation in the normal direction while Fig. 9 (c), (d), (e) and (f) show the response of the sensor when the palpation moved along the breast in the southeast, northeast, northwest and southwest directions, respectively. We see that in each case, the sensor was able to follow the path of motion, which is shown in Fig. 9 (g). The clear differences in each of the individual signal patterns allowed us to differentiate between different directions and hence track the trajectory of motion of the hand as it moved around the breast during the examination.

## VI. Conclusion

In conclusion, this paper reports a flexible, rapidly prototypable, capacitive touch-force sensor with a novel patterned dielectric layer and operation of the sensor and described the fabrication of the devices using photolithography along with soft-lithography using 3D printed molds. As a result, we were able to rapidly fabricate and prototype these sensors based on the specific application requirements. We performed 3D, coupled-multiphysics simulations in ANSYS in order to analyse the effects of the variations in the dielectric post geometries on the mechanical and electronic properties of the sensors. The experimental data was in agreement with these results and show that this sensor is capable of discerning between motion in different directions and furthermore, is able to follow the trajectory of motion that was applied to a model breast. This would validate the use of such a sensor as a CBE training tool for residents.

The resulting sensors are flexible, extremely sensitive, robust and invariant to temperature changes and show low levels of hysteresis. We envision applications in the areas of prosthetics shear measurement, haptic and robotic tactile sensing. The device can be tailored to meet the demands of various applications by changing the substrate material, dielectric layer patterns and electrode geometries. There is much that can be done to improve the performance of the sensor. Future work would involve improving the fabrication process in order to improve the dielectric post alignment, developing an in-house system that can better actuate and characterize the sensor, designing a multiplexed array of the sensors and developing algorithms for analyzing signal patterns to predict the type and direction of motion. In addition, improving the mechanical and electrical interfaces to the readout circuit, optimizing the electrode geometry to improve shear sensitivity and selecting polymers with higher dielectric constants are possible ways to reduce parasitics and increase the operating capacitance range of the sensor.

## Acknowledgment

The authors would like to thank Dr. Carla M. Pugh and Dr. Shlomi Laufer for their early support in this project. They would also like to thank Mark Allie for providing us with access to his lab, and Dr. Yen-Sheng Lu, Abi Seshadri and Kari Van Grinsven for discussion.

## REFERENCES


[1] A. L. Siu, "Screening for breast cancer: U.S. Preventive services task force recommendation statement," *Ann. Int. Med.*, vol. 164, no. 4, pp. 279–296, 2016.

[2] R. G. Miller, "Breast cancer screening," *J. Gen. Internal Med.*, vol. 16, no. 3, pp. 206–207, Mar. 2001. [Online]. Available: https://doi.org/10.1111/j.1525-1497.2001.10119.x, doi: 10.1111/j.1525-1497.2001.10119.x.

[3] M. B. Barton, S. W. Fletcher, and R. Harris, "Does this patient have breast cancer? The screening clinical breast examination: Should it be done? How?" *JAMA*, vol. 282, no. 13, pp. 1270–1280, Oct. 1999.

[4] S. McDonald, D. Saslow, and M. H. Alciati, "Performance and reporting of clinical breast examination: A review of the literature," *CA Cancer J. Clin.*, vol. 54, no. 6, pp. 345–361, 2004.

[5] J. Chalabian, S. Formenti, C. Russell, J. Pearce, and G. Dunnington, "Comprehensive needs assessment of clinical breast evaluation skills of primary care residents," *Ann. Surg. Oncol.*, vol. 5, no. 2, pp. 166–172, 1998.

[6] C. A. Kotwall, "Assuring competency in clinical breast evaluation skills," *Amer. J. Surg.*, vol. 176, no. 6, p. 678, 1998.

[7] D. C. Hall, C. K. Adams, G. H. Stein, H. S. Stephenson, M. K. Goldstein, and H. S. Pennypacker, "Improved detection of human breast lesions following experimental training," *Cancer*, vol. 46, no. 2, pp. 408–414, 1980.

[8] K. M. Freund, R. B. Burns, and L. Antab, "Improving residents' performances of clinical breast examination," *J. Cancer Edu.*, vol. 13, no. 1, pp. 20–25, 1998.

[9] S. Laufer *et al.*, "Sensor technology in assessments of clinical skill," *New England J. Med.*, vol. 372, no. 8, pp. 784–786, 2015.

[10] C. Kwan, L. Salud, E. Cohen, and C. Pugh, "Validity of a newly developed tri-axial sensor for clinical breast examination skills assessment," *Stud. Health Technol. Inf.*, vol. 196, pp. 225–229, Jan. 2014.

[11] C.-C. Chiang, C.-C. K. Lin, and M.-S. Ju, "An implantable capacitive pressure sensor for biomedical applications," *Sens. Actuators A, Phys.*, vol. 134, no. 2, pp. 382–388, 2007.

[12] A. Charalambides and S. Bergbreiter, "A novel all-elastomer MEMS tactile sensor for high dynamic range shear and normal force sensing," *J. Micromech. Microeng.*, vol. 25, no. 9, p. 095009, 2015.

[13] S. Miller and Z. Bao, "Fabrication of flexible pressure sensors with microstructured polydimethylsiloxane dielectrics using the breath figures method," *J. Mater. Res.*, vol. 30, no. 23, pp. 3584–3594, 2015.

[14] B. Li, Y. Shi, H. Hu, A. Fontecchio, and Y. Visell, "Assemblies of microfluidic channels and micropillars facilitate sensitive and compliant tactile sensing," *IEEE Sensors J.*, vol. 16, no. 24, pp. 8908–8915, Dec. 2016.

[15] H. K. Lee, J. Chung, S. I. Chang, and E. Yoon, "Normal and shear force measurement using a flexible polymer tactile sensor with embedded multiple capacitors," *J. Microeletromech. Syst.*, vol. 17, no. 4, pp. 934–942, 2008.

[16] J. Fernandes and H. Jiang, "Three axis capacitive touch sensor for clinical breast examination training," in *Proc. IEEE SENSORS*, Oct./Nov. 2016, pp. 1–3.

[17] C.-C. Huang, X. Wu, H. Liu, B. Aldalali, J. A. Rogers, and H. Jiang, "Large-field-of-view wide-spectrum artificial reflecting superposition compound eyes," *Small*, vol. 10, no. 15, pp. 3050–3057, 2014.

[18] X. Zeng and H. Jiang, "Polydimethylsiloxane microlens arrays fabricated through liquid-phase photopolymerization and molding," *J. Microelectromech. Syst.*, vol. 17, no. 5, pp. 1210–1217, Oct. 2008.

[19] M. J. Moghimi, J. Fernandes, A. Kanhere, and H. Jiang, "Micro-Fresnel-zone-plate array on flexible substrate for large field-of-view and focus scanning," *Sci. Rep.*, vol. 5, p. 15861, Oct. 2015.

[20] C. Li and H. Jiang, "Fabrication and characterization of flexible electrowetting on dielectrics (EWOD) microlens," *Micromachines*, vol. 5, no. 3, pp. 432–441, 2014.

[21] Y.-S. Lu, H. Tu, Y. Xu, and H. Jiang, "Tunable dielectric liquid lens on flexible substrate," *Appl. Phys. Lett.*, vol. 103, no. 26, p. 261113, 2013.


**Jayer Fernandes** received the B.E. degree in electronics and communications engineering from the Visvesvaraya Technological University, Karnataka, India, in 2009, and the M.S. degree in electrical and computer engineering from the University of Wisconsin–Madison, Madison, WI, USA in 2014, where he is currently pursuing the Ph.D. degree with the Department of Electrical and Computer Engineering. His research focuses on the development of flexible tactile sensors for different biomedical applications. His other research interests include flexible optical sensors and micro-optics.

**Hongrui Jiang** (S'98–M'02–SM'10–F'17) received the B.S. degree in physics from Peking University, Beijing, China, and the M.S. and Ph.D. degrees in electrical engineering from Cornell University, Ithaca, NY, USA, in 1999 and 2001, respectively. From 2001 to 2002, he was a Post-Doctoral Researcher with the Berkeley Sensor and Actuator Center, University of California at Berkeley. He is currently the Vilas Distinguished Achievement Professor and the Lynn H. Matthias Professor of Engineering with the Department of Electrical and Computer Engineering, a Faculty Affiliate with the Department of Biomedical Engineering, the Department of Materials Science and Engineering, and the Department of Ophthalmology and Visual Sciences, and a member of the McPherson Eye Research Institute, University of Wisconsin–Madison. His research interests are in microfabrication technology, biological and chemical microsensors, microactuators, optical microelectromechanical systems, smart materials and micro-/nano-structures, lab-on-chip, and biomimetics and bioinspiration. He is a member of the Editorial Board of the IEEE/ASME JOURNAL OF MICROMECHANICAL SYSTEMS.

Dr. Jiang is a Fellow of the Institute of Physics, the Royal Society of Chemistry, the American Institute for Medical and Biological Engineering, and the Institute of Electrical and Electronics Engineers. He was a recipient of the National Science Foundation CAREER Award and the Defense Advanced Research Projects Agency Young Faculty Award in 2008, the H. I. Romnes Faculty Fellowship of the University of Wisconsin–Madison in 2011, the National Institutes of Health Directors New Innovator Award in 2011, the Vilas Associate Award of the University of Wisconsin in 2013, and the Research to Prevent Blindness Stein Innovation Award in 2016.